Journal of Power Sources 193 (2009) 607–616

Contents lists available at ScienceDirect

Journal of Power Sources

journal homepage: www.elsevier.com/locate/jpowsour

Effect of various coal contaminants on the performance of solid oxide fuel cells: Part I. Accelerated testing

JianEr Bao*, Gopala N. Krishnan, Palitha Jayaweera, Jordi Perez-Mariano, Angel Sanjurjo

SRI International, 333 Ravenswood Ave, Menlo Park, CA 94025, USA

ARTICLE INFO

Article history:
Received 3 February 2009
Received in revised form 12 April 2009
Accepted 15 April 2009
Available online 3 May 2009

Keywords:
Solid oxide fuel cell
Poisoning
Fuel contaminants
Coal syngas
Performance degradation

ABSTRACT

The contaminants that are potentially present in the coal-derived gas stream and their thermochemical nature are discussed. Accelerated testing was carried out on Ni–YSZ/YSZ/LSM solid oxide fuel cells (YSZ: yttria stabilized zirconia and LSM: lanthanum strontium manganese oxide) for eight main kind of contaminants: CH_3Cl, HCl, As, P, Zn, Hg, Cd and Sb at the temperature range of 750–850 °C. The As and P species, at 10 and 35 ppm, respectively, resulted in severe power density degradation at temperatures 800 °C and below. SEM and EDX analysis indicated that As attacked the Ni region of the anode surface and the Ni current collector, caused the break of the current collector and the eventual cell failure at 800 °C. The phosphorous containing species were found in the bulk of the anode, they were segregated and formed "grain boundary" like phases separating large Ni patches. These species are presumably nickel phosphide/phosphate and zirconia phosphate, which could break the Ni network for electron transport and inhibit the YSZ network for oxygen ion transport. The presence of 40 ppm CH_3Cl and 5 ppm Cd only affected the cell power density at above 800 °C and Cd caused significant performance loss. Whereas the presence of 9 ppm Zn, 7 ppm Hg and 8 ppm Sb only degraded the cell power density by less than 1% during the 100 h test in the temperature range of 750–850 °C.

1. Introduction

The U.S. Department of Energy's Solid State Energy Conversion Alliance (SECA) program envisions the development of high-efficiency, low-emission, CO_2 sequestration-ready and fuel-flexible technologies to produce electricity from fossil fuels. One such technology is the integrated coal gasification-solid oxide fuel cell (SOFC) that produces electricity from the gas stream of a coal gasifier. SOFCs have high, direct fuel-to-electricity conversion efficiencies of 45–50% (with the total efficiency of more than 80% when the cogenerated heat is also employed), environmental compatibility (low NO_x production) and modularity, and no need for the high cost precious metal use. However, commercialization of this technology is not readily available, due to the naturally occurring coals having many impurities and some of these impurities end in the fuel gas stream either as a vapor phase or in the form of fine particulate matter even after the gas stream cleanup process, thus cause the performance degradation of the SOFCs. Establishing the tolerance limits of the SOFCs for various contaminants in the coal-derived gas will allow proper design of the fuel feed system that will not catastrophically damage the SOFCs or allow long-term cumulative degradation, and to avoid of unfavorable operating conditions.

Currently, porous Ni–YSZ (yttria stabilized zirconia) cermet is the most widely used anode material for SOFC application because of its high catalytic activity, low cost, and high chemical and mechanical stability in reducing atmosphere at high temperature [1]. However, this type of anodes is usually vulnerable to degradation in the presence of contaminants that are expected to be present in a coal-derived fuel gas stream. Different contaminants in the fuel stream can lead to different types of performance degradation depending on the impurity's thermochemical nature, concentration level, and mechanism of poisoning. They can block the reactive surface sites of the nickel particles in the anode deteriorating the catalytic ability (surface effect); react with the YSZ network impeding the transportation of the oxygen ions (bulk effect); and change the morphology of the nickel particle–YSZ network bringing down the electrical conductivity.

Though a significant level of effort has been invested, concentrations of many trace contaminants in coal-derived gas streams are still not known accurately. The expected levels depend on the type of coal, coal gasifier, and gas stream cleanup technology. Both warm gas cleanup and cold gas cleanup technologies are being investigated to remove the contaminants from the coal gas. The warm gas cleanup systems (>200 °C) preserve the enthalpy of steam condensation and are expected to reduce H_2S,

* Corresponding author.
E-mail address: valeriebao@gmail.com (J. Bao).

0378-7753/$ – see front matter © 2009 Elsevier B.V. All rights reserved.
doi:10.1016/j.jpowsour.2009.04.034

HCl, and other major contaminants to ppm levels. The cold gas cleanup systems such as absorption in Selexol (polyethylene glycol ethers) or Rectisol (methanol) that are in commercial use operate at ambient or sub-ambient temperatures and have the ability to remove the impurities to sub-ppm levels (with higher cost, however). The best data available so far are from a process that is being used for the production of methanol from coal-derived gas at the Eastman Chemical Company's chemicals from a coal complex at Kingsport, TN. It indicated that the following contaminants may be present after the coal gas has undergone Rectisol cleanup: AsH_3 = 0.15–0.58 ppm; CH_3Cl = 2 ppm; CH_3SCN = 2.1 ppm; $Fe(CO)_5$ = 0.05–5 ppm; HCl = <1 ppm; $Ni(CO)_5$ = 0.001–0.025 ppm; PH_3 = 1.9 ppm; Sb = 0.025 ppm; and Zn = 9 ppm.

Only a limited number of investigations have been conducted to determine the effect of contaminants in coal-derived gas on the performance of SOFCs. Of these, H_2S has received the most attention, followed by NH_3 and HCl vapor [2]. At 1000 °C, NH_3, at about 5000 ppm levels, did not have a measurable effect to the performance. HCl at 1 ppm level did not affect the performance of the SOFC either, although higher levels were assumed to have long-term effect. A wide range of concentration levels for H_2S (from sub-ppm level to several thousand ppm) has been investigated in the temperature range of 500–1000 °C by several authors [3–12]. The common findings are that ppm level of H_2S causes an immediate drop of cell power density, and the performance degradation is less severe at higher temperatures than at lower temperatures. Controversies exist regarding to whether the power density remains constant after the initial degradation or continues to decrease and the mechanism for the cause of degradation.

A few studies have reported the effect of potential contaminants in a coal-derived fuel gas on the performance of SOFC using a simulated gas stream under laboratory conditions. In the temperature range of 800–900 °C, the presence of HCl vapor (20–160 ppm) caused performance losses in the SOFCs that increased with temperature and the amount of HCl vapor present [13]. Haga et al. [12] reported that formation and vaporization of $NiCl_2$ nanoparticles occurred with an anode gas containing 100 and 1000 ppm of $Cl_2(g)$ in $H_2(g)$ at 800 °C.

Marina et al. [14] reported that anode degradation occurred in the presence of PH_3 and the degradation is irreversible due to the formation of Ni_5P_2 phase. Researchers at West Virginia University [15] have shown that a Ni–YSZ anode had a reduced porosity after exposure to 20 ppm PH_3 at 900 °C and the phosphorous species had reacted with Ni and Zr, leading to the formation of $Ni_3(PO)_4$ and ZrP_2O_7.

The performance of solid oxide fuel cells (SOFCs) using simulated coal-derived syngas containing arsine (AsH_3) was studied by Trembly et al. [16]. The tests with simulated coal syngas containing 1 ppm AsH_3 show little degradation over 100 h of operation. The tests with simulated coal syngas containing 2 ppm AsH_3 show some signs of degradation, however, no secondary arsenide phases were found. Extended trial testing with 0.1 ppm AsH_3 showed degradation as well as the formation of a secondary nickel arsenide phase in the anode of the SOFC. Gerdes et al. [17] studied the performance of an anode-supported SOFC in a simulated coal gas containing 0.5 and 5 ppm levels of H_2Se. The introduction of 0.5 ppm H_2Se caused the power density to be degraded steadily. Increasing the H_2Se concentration to 5 ppm leads to a significant loss of the power density of ~25% after 75 h of exposure.

Much still remains unclear or even unknown of the poisoning effects by the various impurities present in the coal-derived gas stream. We are not aware of any published study that documents the performance of solid oxide fuel cells in a gas stream from an operating coal gasifier. FuelCell Energy tested a molten carbonate fuel cell stack at the Destec gasifier site [18]. The test included 1500 h of operation using 9142 kJ m^{-3} syngas from a slip stream of a 2180 tonne day^{-1} Destec entrained gasifier. The fuel processing system incorporated cold gas cleanup for bulk removal of H_2S and other contaminants. The test showed that it is feasible to operate a fuel cell from a clean fuel gas stream from a coal gasifier. Recently, FuelCell Energy also tested several 10 kW SOFC stacks for over 5000 h [19]. The performance was expected to meet the DOE 5000 h metric test requirements. But the fuel used was simulated (with a mixture of natural gas, hydrogen, steam, and nitrogen), not directly from a gasifier.

Therefore, the primary objectives of this project are to determine the sensitivity of the performance of the SOFCs to the trace level contaminants most probably present in a coal-derived gas stream in the temperature range of 700–900 °C, and investigate the possible mechanisms for the performance degradation or cell failure. This manuscript discusses the initial accelerated test results, where the contaminant levels are set at relatively high levels so that their effects can be ascertained in a short period of test time (~100 h). If degradation occurs in the accelerated test for a specific contaminant, long-term tests (~1000 h) are carried out to ascertain whether such effects occur at contaminant levels typical of a clean coal gas stream, and the results will be published in part II and part III to follow.

2. Experimental

2.1. Cell preparation

The SOFC cells procured from InDec B.V., Netherlands are 2.5 cm in diameter and are anode supported with the following characteristics: yttria stabilized zirconia (YSZ) electrolyte thickness: 4–6 μm, NiO–YSZ anode layer thickness: 5–10 μm, a porous anode-supported layer (NiO–YSZ) of 465–555 μm thick, and a porous YSZ/LSM (lanthanum strontium manganese oxide) cathode layer of 30–60 μm thick. The Ni cermet cell is mounted on a zirconia ring (2.9 cm OD, 2.3 cm ID, 2.5 mm thick) with the top exposed surface being the cathode side, using AREMCO 516 high temperature cement. The schematic diagram of the cell test system is shown in Fig. 1. The electrical contacts for the bottom anode side are made with a Ni mesh bonded to the anode with Ni cement slurry, and the Ni mesh is attached to gold wire leads for external contacts. The ring-mounted cell with anode contacts is then sealed to a zirconia plate to which zirconia tubes are cemented to form the gas inlet and outlet. The cathode contacts are made with gold wires bonded to the LSM layer with Pt paint. Additionally, the LSM cathode is painted with platinum paint to improve the lateral electrical conductivity. On each side of the cell, there are two contact leads for current and potential measurement (equivalent to four point

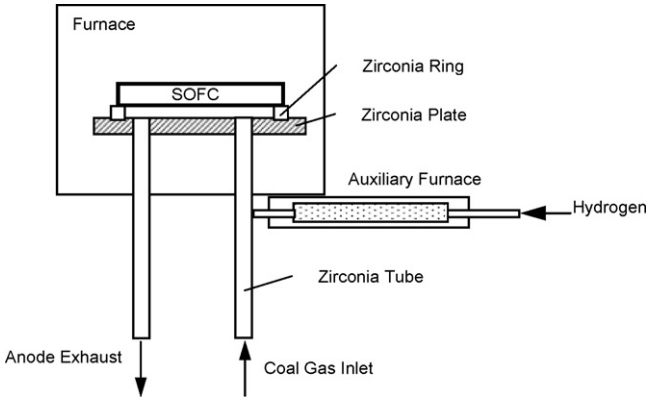

Fig. 1. Schematic diagram of the SOFC test system with a coal gas stream to carry water vapor and a side stream to allow the introduction of contaminant vapor.

measurement), so that the lead resistance in the measurement is eliminated. The active cell area is about 4.5 cm^2. The anode is first heated in air flow to 500 °C at 1 °C min^{-1} and dwells at that temperature for over 10 h to remove the binders in the Ni cement paste, and then the temperature is ramped at 1 °C min^{-1} to the cell test temperature in hydrogen for nickel oxide reduction.

2.2. Fuel delivery and contaminant introduction system

A gas mixture of 46.1% CO, 35.8% H_2, and 18.1% CO_2 is passed through a water stream heated at 70 °C, and carries the water vapor into the cell through the coal gas inlet port shown in Fig. 1. The flow rate of the gas mixture is 65 ml min^{-1}, and the ambient temperature liquid water is injected at a rate of 1.2 ml h^{-1}. Hydrogen flow at around 10 ml min^{-1} is injected to the main coal gas inlet from the side stream port shown in Fig. 1, and then transported together to the anode side of the cell. Contaminants are introduced through this side stream port using H_2 as the carrier gas (in some cases Ar and N_2 are used). The overall flow rate of the fuel gas is approximately 100 ml min^{-1}, and it contains 30.6% H_2, 30.0% CO, 27.6% H_2O, and 11.8% CO_2, simulating the coal-derived gas mixture. The cathode is simply supplied with dry air.

Trace level impurities such as HCl, CH_3Cl, and H_2S are stable gases under ambient conditions, and gas mixtures containing 500 ppm of HCl or CH_3Cl in H_2 from gas supply vendors are procured then. However, for other condensable vapors such as Zn(g), Hg(g), or Cd(g), impurities are introduced by passing a portion of the anode feed gas (H_2 side stream) through a bed of the corresponding metal or oxide maintained at an appropriate temperature which will provide the desired vapor pressure. This H_2 side stream is then maintained at elevated temperature to prevent the vapor re-condensation during fuel transport.

Zinc vapor and cadmium vapor are generated by passing the carrier gas H_2 over a heated bed of Zn and Cd metal powders, respectively. The Zn bed is kept at 380 °C and the corresponding vapor pressure is 5.4×10^{-5} atm (all the vapor pressure data are obtained from Outokumpu HSC Chemistry® software, version 5.1). The carrier gas H_2 is about 18% of the total flow, and the final partial pressure of Zn vapor in the coal gas is approximately 9 ppm. The Cd bed is kept at 278 °C, and the H_2 flow passing through the bed is adjusted so that the Cd contaminant level in the anode gas stream is at 5 ppm.

Mercury vapor and antimony vapor are generated by passing inert carrier gas Ar over a heated bed of HgO powders and Sb_2O_3 powders, respectively. The HgO bed is kept at 273 °C and the corresponding vapor pressure is about 1×10^{-4} atm. Argon is used as the carrier gas so as to keep the oxide bed from being reduced by H_2 or the reducing environment of the coal gas. Whereas for Sb, the stable gaseous species under the anode reducing environment is SbO(g). Therefore, Sb_2O_3 powder bed is used and heated at 476 °C to generate Sb_4O_6(g) at a vapor pressure of 2×10^{-5} atm. When mixed with H_2 at the anode fuel port, it is reduced to SbO(g). The SbO contaminant level tested in this study is 8 ppm.

The nature of the phosphorous compounds in a coal-derived gas stream at the operating conditions of an SOFC is not known accurately. Since the SOFCs operate at 700–900 °C under atmospheric or slightly elevated pressures, the possible form of phosphorous compound PH_3(g) will also be hydrolyzed to HPO_2(g) from thermodynamic equilibrium calculations. Thus P_2O_5 source is used as the vaporizing species. When P_2O_5 powders are heated, they vaporize majorly as P_4O_9(g) and P_4O_{10}(g). The P_2O_5 bed is kept at 127 °C which generates a vapor pressure of 9.8×10^{-5} atm of phosphorous compounds. The H_2 flowing over the P_2O_5 bed is 9% of the total flow and the calculated concentration of P over the anode is about 35 ppm. Note, the volumetric level of phosphorous oxides is about 8.8 ppm, but since the majority of phosphorous oxides vapor contain four P atoms with each molecule, so the concentration level of P is taken to be 35 ppm here.

2.3. Cell testing and characterization

Each cell is first stabilized with the cathode exposed to heated air and the anode in pure H_2 gas until a steady open circuit potential is reached (usually around 1 V at temperatures of 700–900 °C). Then the fuel gas is switched to the simulated coal-derived gas at a flow rate of 100 ml min^{-1}, and an operating current of 1 A (equivalent to 0.222 A cm^{-2}) is loaded to the cell. To establish the baseline performance standard, the cells are first tested in clean simulated coal gas for several hundred hours before each contaminant is introduced. Voltage/power density data are constantly monitored over the period tested, and i–v characteristics are also measured occasionally. If not specially noted, the voltage/power density data are measured with a current load of 1 A (0.222 A cm^{-2}) to the cell.

After testing, secondary electron microscopy (SEM) and energy dispersive X-ray spectroscopy (EDX) analysis are carried out for each cell.

3. Results and discussion

3.1. Clean gas testing

The manufacturer of the fuel cell samples indicates that the cells will be stable within 10% of the original performance over a period of 2000 h under clean gas conditions at 800 °C. To assure such performance and to differentiate the effect of contaminants from that of aging, the performance under clean gas condition is conducted first. In addition, all the tested cells are conditioned for a period of time (~150 h) before the contaminant is introduced into the gas stream.

Fig. 2(a) shows the standard baseline performance of the Ni cermet cell under pure H_2 condition (50 ml min^{-1}) at a current load of 0.222 A cm^{-2}. The maximum power density for the cell in pure H_2 is about 360 mW cm^{-2} at a current density of around 2.5 mA cm^{-2}, and over the 380 h tested, the power density remained constant with the average value being 181 ± 4 mW cm^{-2}. After 388 h, the feed fuel was switched to the coal-derived gas at a flow rate of about 100 ml min^{-1}. The average power density at the same load with this gas mixture is 166 mW cm^{-2}, slightly lower than that with H_2. The cell power density data are noisier in the simulated coal gas, most

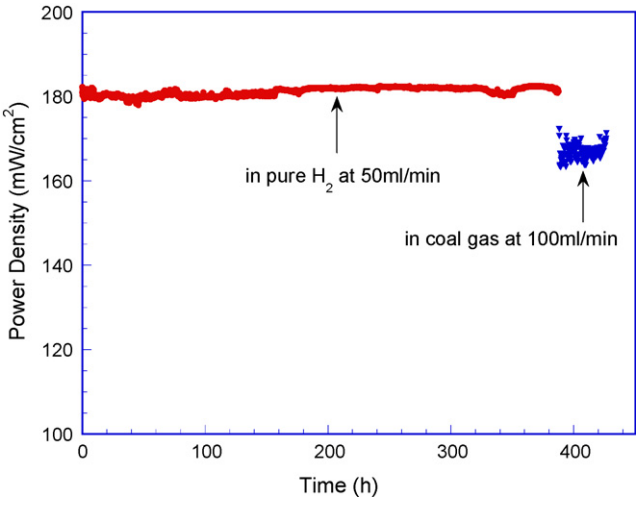

Fig. 2. Baseline performance of the Ni cermet cell at 800 °C with 50 ml min^{-1} H_2 flow at 0.222 A cm^{-2} load for 380 h and then switched to coal gas.

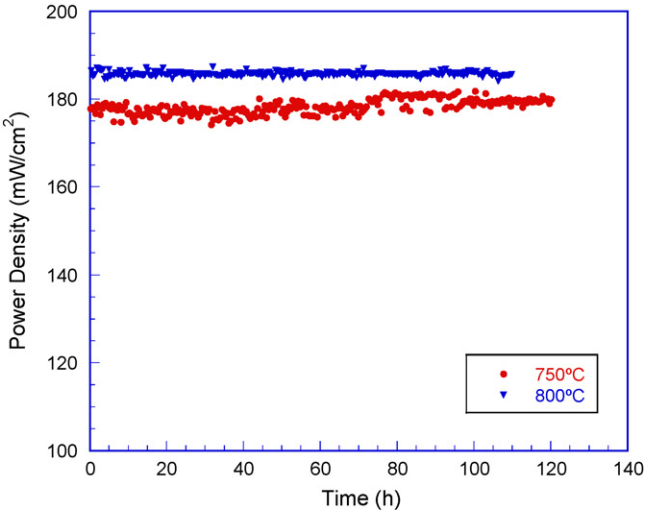

Fig. 3. The variation of the cell power density over time during exposure to 40 ppm HCl gas in simulated coal gas at 750 and 800 °C at a current load of 0.222 A cm^{-2}. Measured average cell voltages are 798 and 835 mV, respectively.

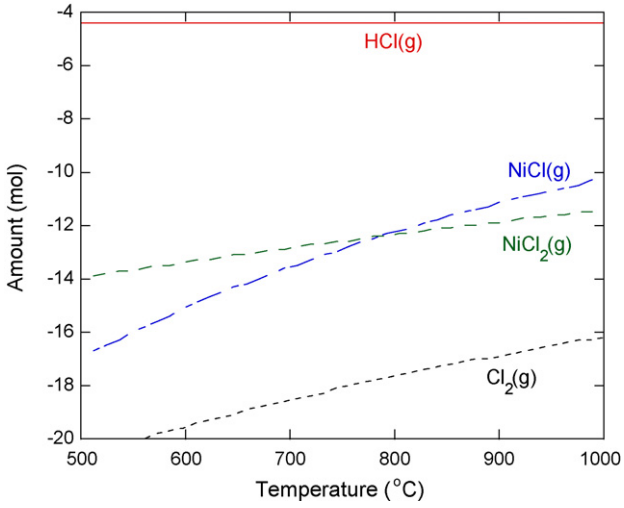

Fig. 5. Phase diagram of chlorine species in Ni–H–Cl–O system as a function of temperature calculated by HSC Chemistry® software. Assuming the amount of Ni is 1 mol, H_2(g) 0.6 mol, H_2O(g) 0.4 mol, and HCl(g) 40 ppm (mol%).

likely due to gas flow fluctuation arising from the steam injection by a syringe pump. As seen from Fig. 2, no noticeable degradation occurred to the cell performance in the test duration. The following discusses the effect of contaminants to the performance of SOFCs and suggests the possible degradation/failure mechanisms. Chlorine compounds (HCl and CH_3Cl) and metalloids (As, P and Sb) are first discussed, followed by vaporizable metals (Zn, Hg and Cd).

3.2. *Effect of HCl(g) and CH_3Cl(g) on the cell performance*

After the cell was stabilized in the simulated clean coal gas mixture, it was exposed to 40 ppm level of HCl(g). As seen from Fig. 3 for the time variation of the cell power density, no significant degradation was observed during the 100 h testing both at 750 and 800 °C. The voltages at the current load level are 798 and 835 mV, respectively.

Fig. 4 shows the time variation of the power density when the cell is exposed to 40 ppm of CH_3Cl(g) at 800 and 850 °C. No noticeable degradation occurred to the cell performance at 800 °C during the exposure within the testing period (~150 h). However, the cell performance started to decrease after about 80 h of exposure at 850 °C, and the power density dropped from 182 to 173 mW cm^{-2} approximately within 60 h (degradation rate: ~0.15 mW cm^{-2} h^{-1}). Note, the cell tested at 850 °C was previously tested at 800 °C.

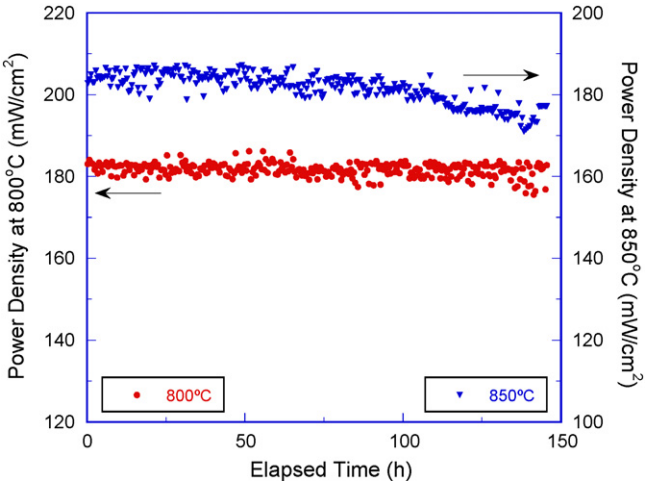

Fig. 4. Time variation of the cell power density when exposed to 40 ppm CH_3Cl(g) at 800 and 850 °C.

Thermochemical calculations indicate that nickel chlorides are not stable in the reducing environment of the coal gas at anode operating temperatures (ΔG of the reaction $Ni + 2HCl = NiCl_2 + H_2$ becomes positive above 450 °C), and the only stable chlorine specie is HCl(g), with significantly less amount of NiCl(g), $NiCl_2$(g), Cl(g), etc. The amount of chlorine species in logarithm scale as a function of temperature for Ni–H–Cl–O system is shown in Fig. 5, calculated by HSC Chemistry® software assuming the amount of HCl(g) in the fuel is 40 ppm (in mol ratio) with 0.6 mol H_2(g) and 0.4 mol H_2O(g). As can be seen, the amount of gas phase chlorine species besides HCl(g) increase as temperature increases. However, even at 1000 °C, the amount is still below 10^{-10} mol for each species. Therefore, it is not likely that the power density degradation after 80 h of exposure to 40 ppm CH_3Cl(g) at 850 °C is due to the loss of Ni catalyst by forming gas phase chlorides and evaporating away. High temperature mass spectrometry (with detection limit of 5×10^{-11} atm) also could not detect any vapor phase of nickel chloride at 800 °C with 400 ppm of CH_3Cl. Haga et al. [12] also studied the poisoning effect of Cl_2(g) to electrolyte supported Ni–ScSZ (scandia stabilized zirconia) cermet anodes. They found that sluggish degradation for the cell performance was observed for hydrogen based, humidified (3% H_2O) fuel containing 5 ppm Cl_2(g), whereas 100 and 1000 ppm Cl_2(g) caused continuous and significant degradation to the performance at 800 °C. From the stability diagram of Ni–O–H–Cl system they calculated thermochemically, it is seen that both solid state and gas phase $NiCl_2$ form at Cl_2 pressures above 10^{-5} and 10^{-6} atm at 1000 and 900 °C, respectively, when the oxygen partial pressure is low. Therefore, they attributed the degradation to the formation (through the reaction $Cl_2(g) + Ni(s) \Leftrightarrow NiCl_2(s, g)$) and evaporation of $NiCl_2$ at the anode. It is very surprising that significant deposits of $NiCl_2$ nanoparticles were found on ScSZ surface in the highly reducing H_2 environment at the cell operating temperature (note, the 5 ppm concentration level in Fig. 4(b) caption in their work may should be changed to 1000 ppm), as thermodynamically, H_2 would react with $NiCl_2$ to form the most stable HCl(g) and Ni. Twigg [6] studied the poisoning effect of CH_3Cl on the catalytic activity of Ni for steam reforming natural gas. He reported that formation of nickel chloride is thermodynamically not favorable under the operating environment, and the chloride poisoning is due to the increasing amount of Cl-containing surface species adsorbed on the surface. To our understanding, it is

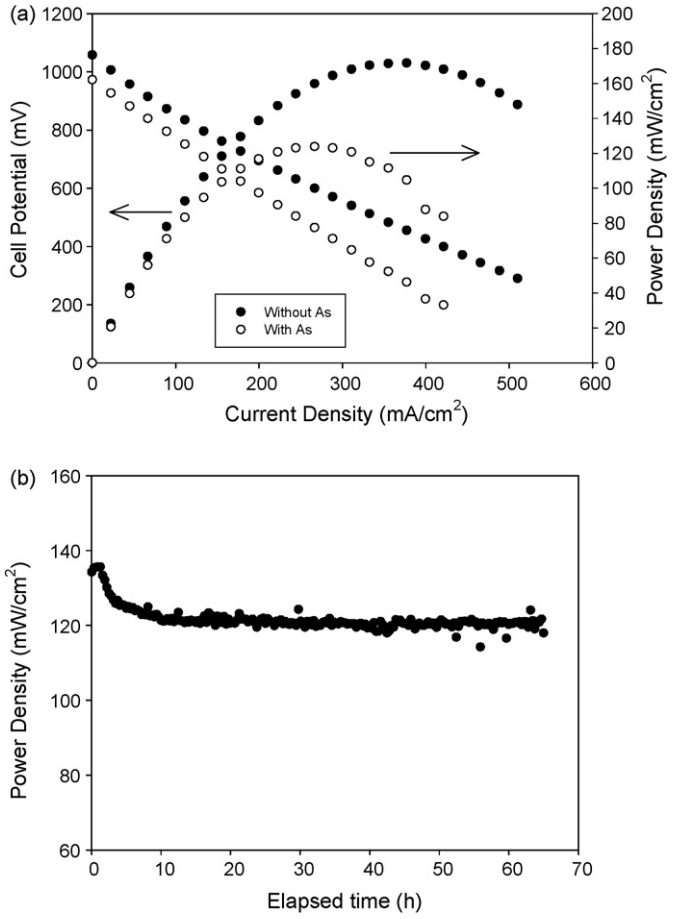

Fig. 6. Cell performance during the exposure to 10 ppm As vapor at 750 °C. (a) *i–v* characteristics before and after the introduction of As and (b) time variation of the power density during the exposure to As.

most likely that the poisoning effect of the chloride is due to some surface adsorption on Ni catalyst, or some bulk effect on the supporting YSZ network. This remains to be solved in the following papers.

3.3. *Effect of arsenic compounds on the cell performance*

The effect of As(g) on the performance of the cell at 750 °C is shown in Fig. 6(a) and (b) as the *i–v* characteristic before and after the introduction of As, and the time variation of the cell power density during the exposure. On the introduction of 10 ppm As(g), the power density of the cell continuously declined during the initial 10 h, and then remained steady over a period of 60 h. Following this test, the cell temperature was increased to 800 °C. At this higher temperature, the cell performance became erratic, see Fig. 7. After a period of 120 h, no current could be drawn from the cell thereby the test was terminated. After the cell was disassembled, it was found that the nickel current collector wires in the anode chamber were loose, brittle and broke easily. The collector wire and the anode were then examined by SEM and EDX analysis to determine the cause of the failure.

Fig. 8(a) shows the surface morphology of the anode surface that was not exposed to any As, and (b) shows the morphology after the exposure to 10 ppm As vapor at 800 °C. Fig. 8(a) clearly shows the network of electrolyte supported Ni anode, with the bright skeleton rich in Zr, and the dark filler rich in Ni. Dramatic surface morphology change is clearly seen with the effect of As exposure. A lot of micrometer size particles are formed at the

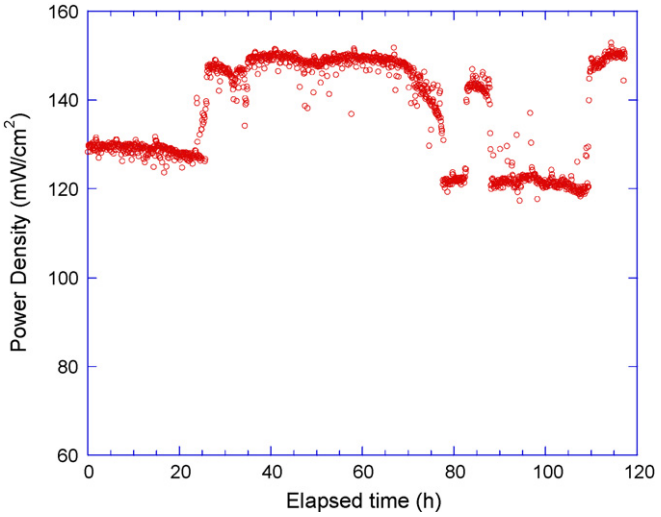

Fig. 7. Time variation of the cell power density during the exposure to 10 ppm As vapor at 800 °C.

anode surface after exposure. Fig. 9 shows the elemental distribution of Ni, As, and Zr for this area by EDX. Note, the top left photograph marked with SE is the secondary electron image. From Fig. 9, it is seen that there is a strong correlation between the Ni and As images, indicating that As is primarily deposited on the

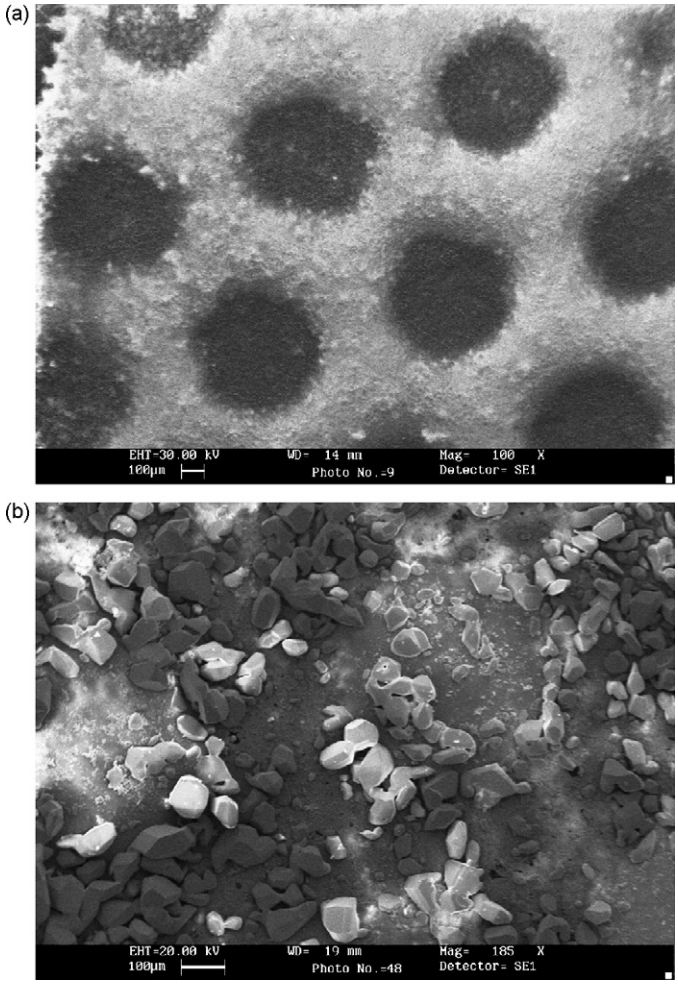

Fig. 8. SEM graphs of the SOFC anode. (a) Not exposed to As and (b) after exposure to 10 ppm As vapor at 800 °C.

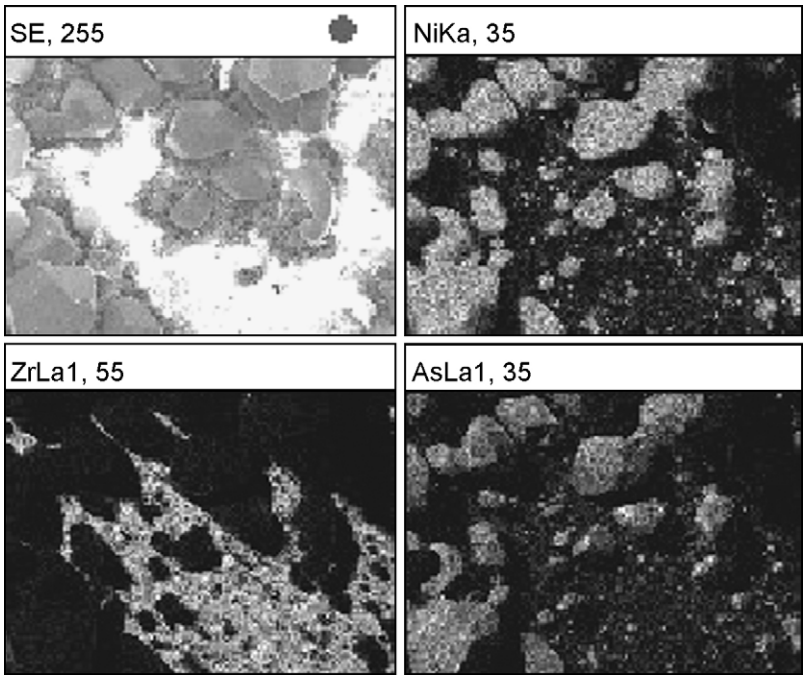

Fig. 9. The X-ray elemental mapping of Ni, Zr, and As for a portion of the SEM graph shown in Fig. 8(b).

Ni granules. The dissolution of As in Ni or the potential formation of nickel arsenides can embrittle the nickel metal screen or the porous nickel layer. These changes can delaminate the current collector from the anode surface leading to erratic cell power densities.

Fig. 10(a) shows the SEM graph of the cross-section of the cell after exposure to 10 ppm As at 800 °C, and (b) is an enlarged view of the highlighted area in figure (a) showing three distinctive layers, being the anode layer, electrolyte, and cathode layer, respectively, from left to right. The cross-section is divided into eight sections from left to right. Section 1 is the top layer of the anode where micro-size crystallites are seen; sections 2–6 are the electrolyte supported Ni cermet anode, section 7 is the YSZ electrolyte, and section 8 is the LSM cathode layer. EDX analysis was done for each section, and the result is shown in Table 1 for the concentration of each element. A gradual increase of Ni amount and decrease of Zr amount are observed in the anode body, as expected. The electrolyte is dominated by Zr, and the cathode is composed of mainly La and Mn. An interesting finding is that As is only found at the anode top, with the concentration level as high as 64.4%. Combining Fig. 9, it is concluded that As likes to deposit on top of Ni and is primarily present on the surface. Since crystallites were observed, it is likely that nickel arsenides were formed.

The formation of nickel arsenides resulted in the current collector being loose and easily broken, and consequently the failure of the cell.

Table 1
EDX analysis for the labeled sections in Fig. 10.

Section	Name	Ni (at.%)	As (at.%)	Zr (at.%)	Mn (at.%)	La (at.%)
1	Anode top	35.6	64.4			
2	Anode	29.4		70.6		
3	Anode	38.6		61.5		
4	Anode	41.1		58.9		
5	Anode	58.4		41.6		
6	Anode	95.6		4.4		
7	Electrolyte	3.3		96.7		
8	Cathode				53.9	42.7

3.4. Effect of phosphorous compounds

Fig. 11 shows the effect of the addition of 35 ppm phosphorous oxides vapor to the cell power density at 750 and 800 °C. At

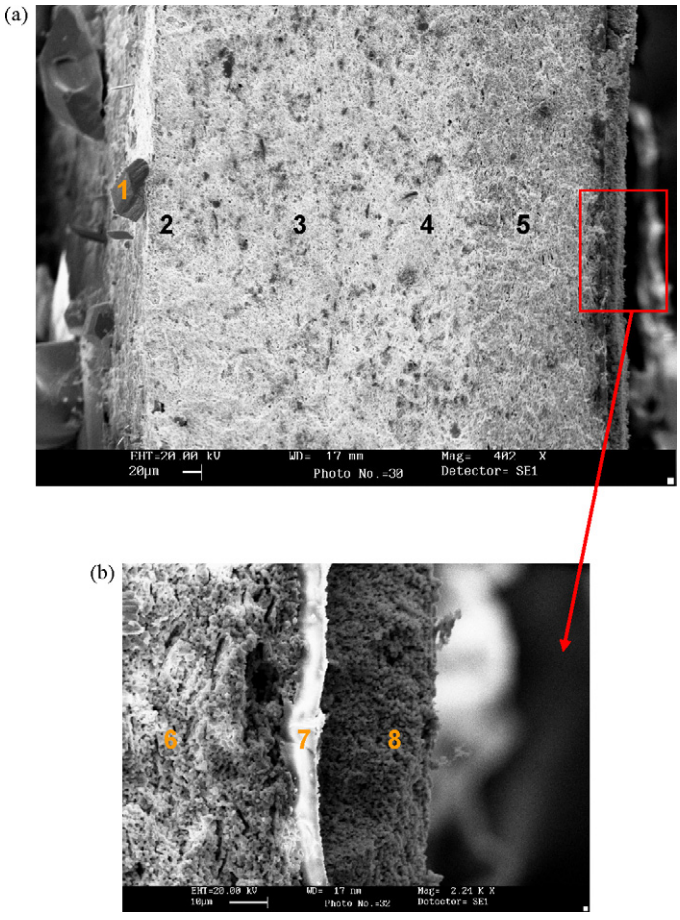

Fig. 10. SEM image of the cross-section of the arsenic contaminated cell.

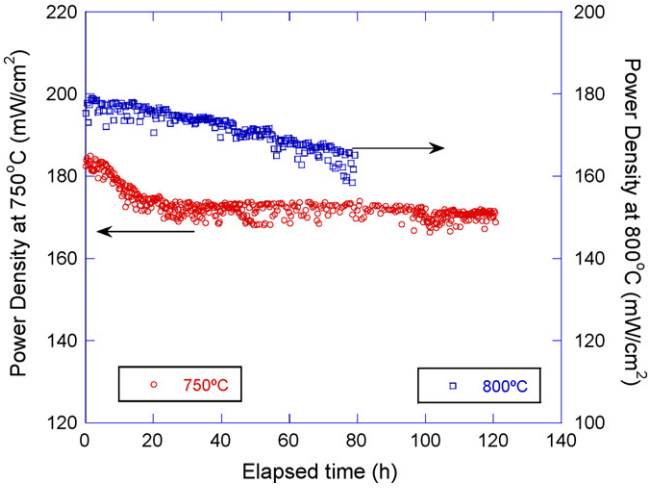

Fig. 11. Time variation of the cell power density during the exposure to 35 ppm phosphorous oxide vapor at 750 and 800 °C. *Note*: the scale of the *Y*-axis is different for two temperatures in order for a clear illustration.

750 °C, the effect is immediately seen: the power density dropped by about 10 mW cm^{-2} within the first 20 h addition. After this initial decay, only a very slow degradation (less than 0.03 mW cm^{-2} h^{-1}) is observed during the next 100 h exposure.

When the temperature is raised to 800 °C, an accelerated degradation to the power density is seen. The average cell degradation rate is about 0.18 mW cm^{-2} h^{-1} during the 80 h exposure, which is a serious poison for the SOFC.

According to the published Ni–P phase diagram [20], the solubility of P in Ni is very limited, e.g. only 0.17 wt% at 870 °C. Even within such low solubility limit, the P atoms tend to segregate to the surface. If the HPO_2(g) decomposes at Ni surface and reacts with Ni, assume P was added to the anode at a rate of 3.5×10^{-4} g h^{-1}, it is estimated that the solubility limit would be reached after about several tens of hours, assuming that the anode contains 50 wt% of Ni. Because P atoms segregate preferentially to the surface, the majority of P atoms will remain at the surface of the active Ni electrocatalyst, blocking the sites for fuel gas adsorption and dissociation. Whereas, if the HPO_2(g) is not dissociated, it may react with Ni and Zr to form nickel phosphate or zirconia phosphate.

The cell after exposure to phosphorous species was characterized by SEM and EDX methods. Fig. 12(a) shows the surface morphology of the anode top layer after exposure to 35 ppm P. The surface is "etched" by the contaminant, and small, irregular particles are exposed (similar to the grain boundaries), surrounding some relatively intact, large patches (parallel to the grains). Fig. 12(b) shows the elemental mapping of the corresponding anode surface area by EDX analysis. It is seen that the large patches are mainly composed of Ni, and they are surrounded by P/Zr. Because the P *Kα* peak (2.014 keV) is very similar to the Zr *Lα*1 (2.042 keV) peak, distinguish between the X-ray emission peaks of P and Zr at that energy may not be accurate. The observed similarity between Zr and P signals could be just coincidental. But what could be determined is that P did not deposit on top of Ni catalyst, instead, P most likely segregated to the boundaries.

Recent work by Zhi et al. [15] on the poisoning effect of phosphorous containing syngas to the anode performance reported the formation of $Ni_3(PO_4)_2$ and ZrP_2O_7 phosphates using XRD analysis after exposing the anode in 20 ppm PH_3(g) at 900 °C. At the open circuit condition, both phosphates were found, whereas at the DC bias of 0.7 V, only nickel phosphate was found at the exposed anode. Combining with our findings, it is likely that the phosphorous containing species preferentially segregated and accumulated into a "grain boundary" like phase (either nickel or zirconia phosphate, or

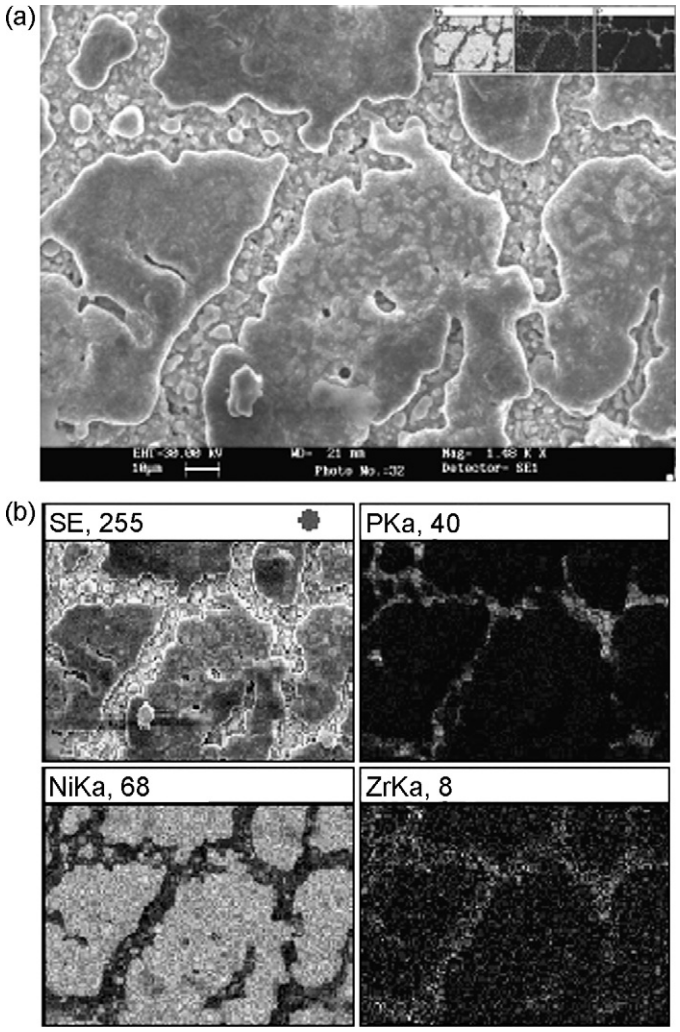

Fig. 12. Surface morphology of the cell after exposure to 35 ppm P. (a) SEM graph and (b) X-ray elemental map of the anode top layer. *Note*: the similarity between P and Zr signals are coincidental because the P *Kα* line coincides with Zr *Lα*1 line.

both), which can break the interconnectivity of the Ni electrocatalyst network for electron transport, and also inhibit the transport of oxygen ions through the YSZ network, resulting in the performance degradation (as also demonstrated by impedance analysis [15] that both the charge transfer resistance and the diffusion resistance increased during exposure). Point analysis by EDX for the distribution of P along the cross-section of the cell also indicated a general trend of the amount of P gradually diminishing from the top anode surface toward the anode/electrolyte interface (with point analysis, the detector setting can be made more precisely to distinguish the P *Kα* peak and the Zr *Lα*1 peak).

3.5. Effect of antimony compounds

Antimony, at level of 8 ppm, was introduced to the syngas to test the poisoning effect to the cell at 750, 800, and 850 °C at a current load of 0.3 A cm^{-2}. No degradation occurred to the cell power density at 750 °C within 100 h exposure, and the *i*–*v* characteristics only showed a very slight decline at very high current levels. At 800 and 850 °C, only slight degradation was observed with a rate at 0.03 mW cm^{-2} h^{-1} (within 160 h) and 0.04 mW cm^{-2} h^{-1} (within 120 h), respectively. Thermodynamic calculations showed that it is possible for Sb to react with Ni and form a NiSb alloy at high temperatures. However, the conversion ratio is not high (~3.5%) [16].

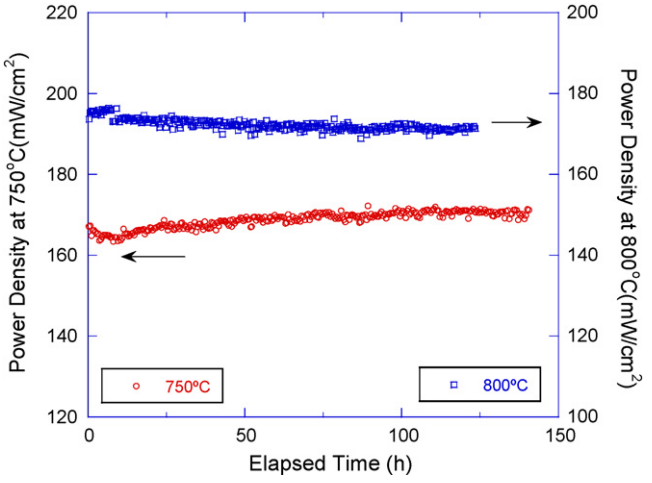

Fig. 13. Time variation of the cell power density during exposure to 9 ppm Zn vapor in a simulated coal gas at 750 and 800 °C.

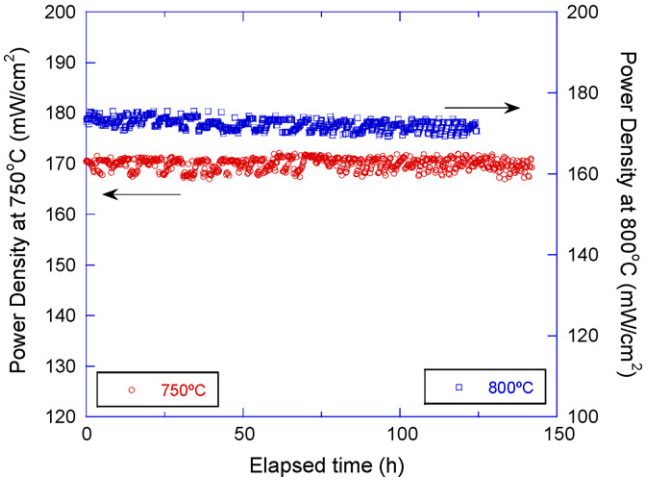

Fig. 14. Time variation of the cell power density during the exposure to 7 ppm Hg vapor at 750 and 800 °C.

At the typical level in the coal-derived gas, Sb would probably not cause significant degradation to the cell performance.

3.6. Effect of Zn vapor

Fig. 13 illustrates the variation of the cell power density as a function of time during the exposure to 9 ppm of Zn vapor at 750 and 800 °C. At 750 °C, no decline in the power density was observed for the 150 h tested. Instead, a slight increase was seen at the initial period of exposure. At 800 °C, only a very slow decline ($\sim$0.025 mW cm^{-2} h^{-1}) occurred continuously over the time of exposure.

Zn is highly soluble in Ni metal at elevated temperatures. At 800 °C, the solubility of Zn in Ni is reported to be $\sim$35 wt% according to the Ni–Zn phase diagram [20]. During the total test period of $\sim$270 h (the cell is first tested at 750 °C for about 150 h, and then the temperature is raised to 800 °C for further exposure), even if all the Zn vapor deposited at the anode (In fact, Zn vapor may be carried over the anode surface without deposition), the amount of Zn added to the anode is still much less than 1% of the nickel present at the anode. At this low level, the added Zn would have dissolved in the Ni matrix. If the dissolved Zn does not segregate to the surface, then electrocatalytic activity of the Ni anode may not change significantly due to Zn addition.

3.7. Effect of HgO vapor

Figs. 14 and 15 illustrate the effect of 7 ppm Hg vapor to the cell power density at 750 and 800 °C. At 750 °C, there was no decline to the power density during the 150 h exposure, and the i–v characteristics in Fig. 15(a) before and after the exposure were almost identical. At 800 °C, a very slow degradation was observed at a rate of 0.02 mW cm^{-2} h^{-1}, as was also demonstrated in Fig. 15(b) at high current densities. Long duration tests and sub-ppm level exposure are necessary to quantify the extent of degradation, which will be published in a later paper.

3.8. Effect of Cd vapor

The effect of 5 ppm Cd vapor to the cell performance is tested at 800 and 850 °C, as vaporizable metals seem to be more deleterious to the anode at higher temperatures. Figs. 16 and 17 show the time variation of the cell performance during the exposure and the i–v characteristics before and after exposure, respectively. From the figures, it is seen that at 800 °C, no degradation occurred to the cell power density at 0.222 A cm^{-2} current load within the 150 h exposure, but the i–v characteristic indicated that some degree of degradation occurred at higher current levels. Whereas at 850 °C, significant degradation was observed after 50 h exposure, and the data became more scattered.

The cell after test was characterized by SEM and EDX methods. The anode morphology remained almost the same, and no

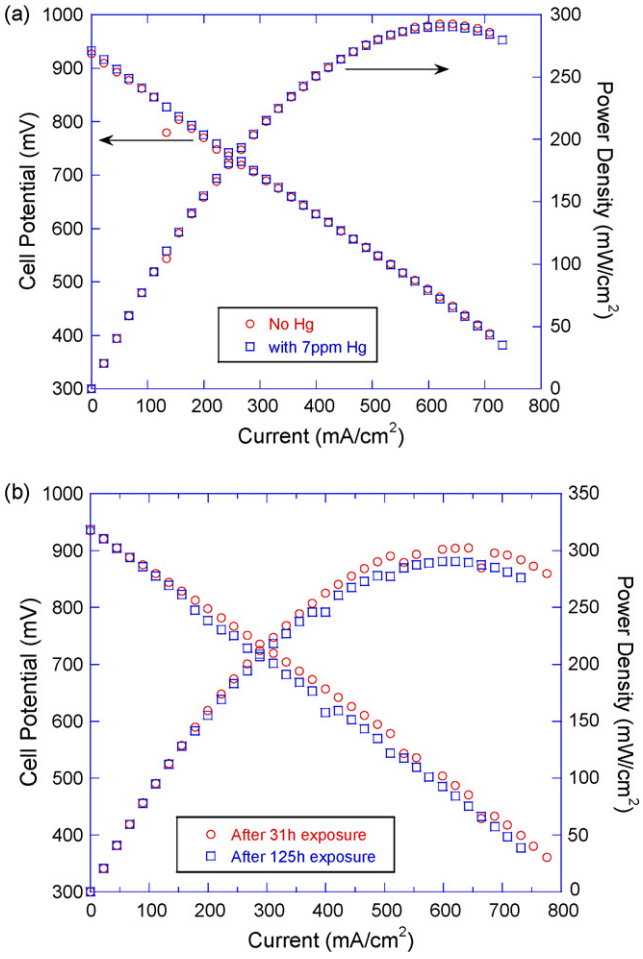

Fig. 15. i–v characteristic of the cell before and after exposure to 7 ppm Hg vapor. (a) At 750 °C and (b) at 800 °C.

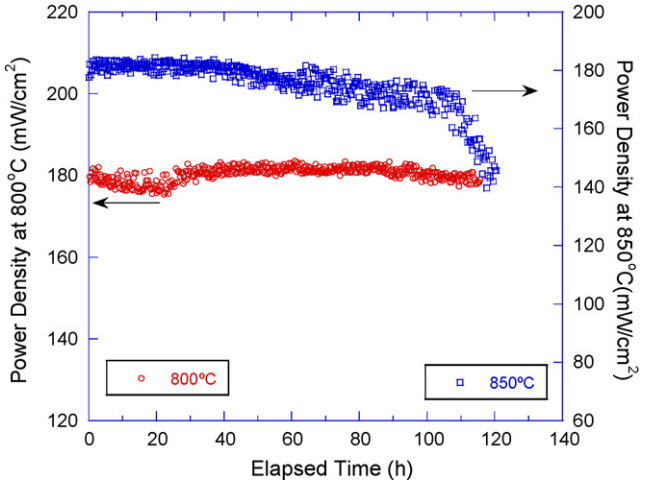

Fig. 16. Time variation of the cell power density during the exposure to 5 ppm Cd vapor at 800 and 850 °C.

detectable level of Cd was found at the anode surface, Ni current collecting mesh and wires, or along the cross-section of the cell. Cd is a very volatile metal, and has vapor pressures of over 10^{-3} Torr at temperatures over 500 K and 10^{-1} Torr at 600 K [21]. So it might be possible that the deposited Cd had all evaporated away during the

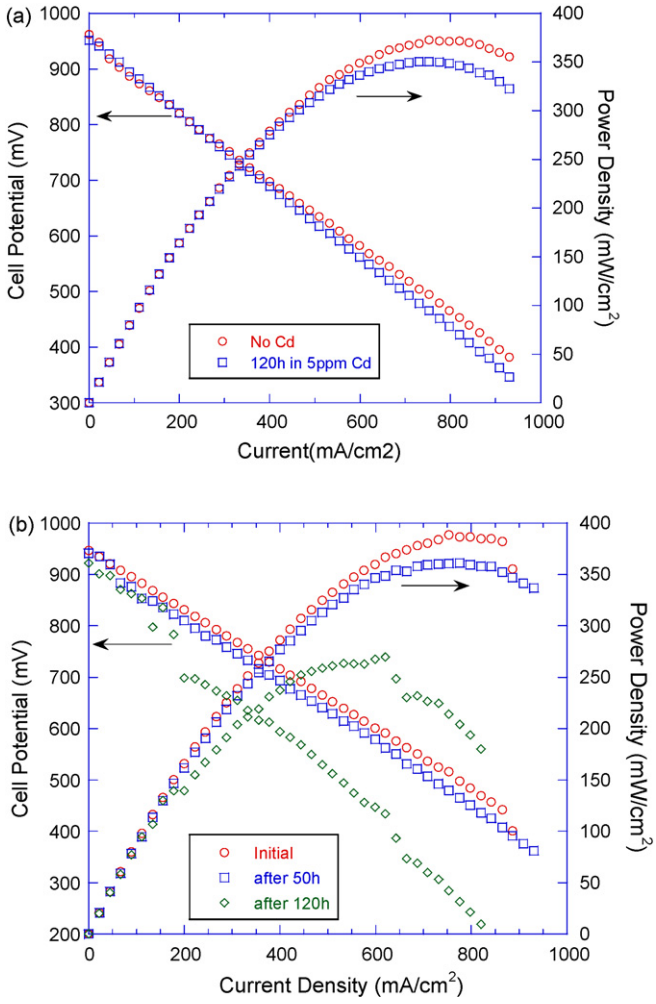

Fig. 17. *i–v* Characteristics of the cell before and after exposure to 5 ppm Cd. (a) At 800 °C and (b) at 850 °C.

Table 2
Degradation of the SOFC power density on exposure to eight coal contaminants.

Contaminant	Exposure Level (ppm)	Degradation (%) with exposure duration		
		750 °C	800 °C	850 °C
As (As_2(g))	10	10 (70 h)	Cell failure[a]	
P (HPO_2(g))	35	7 (120 h)	7.5 (80 h)	
Cd(g)	5		<1 (120 h)	>20 (120 h)
CH_3Cl(g)	40		<1 (150 h)	5 (60 h)
HCl(g)	40	<1 (120 h)	<1 (110 h)	
Hg(g)	7	<1 (150 h)	1.4 (130 h)	
Sb (SbO(g))	8	<1 (100 h)	2 (160 h)	2 (120 h)
Zn(g)	9		<1 (150 h)	1.5 (120 h)

[a] The cell exhibited intermittent performance and failed after 120 h exposure.

slow cooling down period in pure H_2. Goldsmidt and Walker [22] found the formation of secondary Cd phases at Ni rich regions at 800 °C when studying the Ni–Cd system. If Ni is taken by Cd, the fuel adsorption/dissociation process would be affected, and the Ni catalytic activity would be impaired. At the typical concentration level in the coal-derived gas, Cd may cause long-term poisoning effect to the Ni based cermet anode. Further investigation is needed.

4. Summary

In the present work, eight potential contaminants that can be present in the anode feed gas from a coal gasifier were tested at relatively high concentration levels and short exposure duration (accelerated test). Their poisoning effects are summarized in Table 2 in the form of degradation percentage of the power density with the duration of exposure. Among these contaminants tested, As and P species are most likely to degrade the performance at temperatures 800 °C and below. Both these species resulted in severe degradation in the observed cell power density with time of exposure. The As was found mainly at the surface of the Ni cermet anode, attacking the Ni current collector causing electrical connectivity problems and eventual cell failure. The P species were found to be present in the bulk of the Ni cermet anode, and caused significant surface morphology change. Phosphorous containing species (presumably nickel phosphide/phosphate and zirconia phosphate) were segregated and formed "grain boundary" like phase separating large Ni patches. These phosphates could break the interconnectivity of the Ni network for electron transport, and also inhibit the transport of oxygen ions through the YSZ network.

The presence of CH_3Cl(g) and Cd(g) affected the cell power density only at temperatures above 800 °C. Significant power density loss was found during the exposure to 5 ppm Cd(g) at 850 °C. Other vaporizable metallic contaminants such as Hg(g) and Zn(g), and metalloid SbO(g) only resulted in less than 1% degradation over the time tested in the temperature range of 750–850 °C.

Acknowledgement

The authors would like to thank DOE for their financial supporting through the Contract No.: DE-FC26-05NT42627.

References

[1] W.Z. Zhu, S.C. Deevi, Mater. Sci. Eng. A 362 (2003) 228–239.
[2] EG&G Technical Services, Fuel Cell Handbook, 6th edition, DOR/NETL, 2002, p. 1179.
[3] W. Feduska, A.O. Isenberg, J. Power Sources 10 (1983) 89–102.
[4] S.C. Singhal, R.J. Ruka, J.E. Bauerle, C.J. Spengler, Anode Development for Solid Oxide Fuel Cells, Report No. DOE/MC/22046-2371, 1986.
[5] S.C. Singhal, K. Kendall, High Temperature Solid Oxide Fuel Cells: Fundamentals, Design and Applications, Elsevier, Oxford, England, 2003.
[6] M. Twigg, Catalyst Handbook, 2nd edition, Manson Publishing Ltd, London, England, 1996.
[7] Y. Matsuzaki, I. Yasuda, Solid State Ionics 132 (2000) 261–269.

[8] K. Sasaki, K. Susuki, A. Iyoshi, M. Uchimura, N. Imamura, H. Kusaba, Y. Teraoka, H. Fuchino, K. Tsujimoto, Y. Uchida, N. Jingo, J. Electrochem. Soc. 153 (2006) A2023–A2029.
[9] J.P. Trembly, A.I. Marquez, T.R. Ohrn, D.J. Bayless, J. Power Sources 158 (2006) 263–273.
[10] Z. Cheng, M. Liu, Solid State Ionics 178 (2007) 925–935.
[11] J.N. Kuhn, N. Lakshminarayanan, U.S. Ozkan, J. Mol. Catal. A: Chem. 282 (2008) 9–21.
[12] K. Haga, S. Adachi, Y. Shiratori, K. Itoh, K. Sasaki, Solid State Ionics 179 (2008) 1427–1431.
[13] J.P. Trembly, R.S. Gemmen, D.J. Bayless, J. Power Sources 169 (2007) 347–354.
[14] O.A. Marina, L.R. Pederson, D.J. Edwards, C.W. Coyle, J. Templeton, M. Engelhard, Z. Zhu, Proceedings of the 8th Annual SECA Workshop, San Antonio, TX, 2007.
[15] M. Zhi, X. Chen, H. Finklea, I. Celik, N.Q. Wu, J. Power Sources 183 (2008) 485–490.
[16] J.P. Trembly, R.S. Gemmen, D.J. Bayless, J. Power Sources 163 (2007) 986–996.
[17] K. Gerdes, J. Trembly, R. Gemmen, Proceedings of the Coal based Fuel Cell Technology: Status Needs and Future Applications, Morgantown, WV, 2007.
[18] EG&G Services, Parsons, Inc., Science Applications International Corporation, Fuel Cell Handbook, 5th edition, Report to U.S. Department of Energy under contract DE-AM26-99FT40575.
[19] H. Ghezel-Ayagh, Proceedings of the 9th Annual SECA Workshop, Pittsburgh, PA, 2008.
[20] ASM International, ASM Handbook, Volume 3: Alloy Phase Diagram, 1992.
[21] R.E. Honig, RCA Rev. 23 (1962) 567.
[22] H.J. Goldsmidt, M.J. Walker, J. Appl. Crystallogr. 2 (1969) 273–281.